Parametrization of a composite attenuation relation for the Dead Sea area based on 3D modeling of elastic wave propagation

by

Adrien Oth[1], Friedemann Wenzel[1], Hillel Wust-Bloch[2], Ellen Gottschämmer[1] and Zvi Ben-Avraham[2]

1) Geophysical Institute, Karlsruhe University, Hertzstr. 16, 76187 Karlsruhe. Germany

2) Department of Geophysics and Planetary Sciences, Tel Aviv University. P.O.B. 39040, Tel Aviv 69978. Israel

Contact: adrien.oth@ecgs.lu (Adrien Oth)

1

ABSTRACT

3D simulations of elastic wave propagation generated by earthquakes with magnitudes between 5.5 and 7.0 are used to parameterize strong ground motion attenuation relations for the Dead Sea Rift (DSR) graben structure. The results show that standard attenuation relations with an isotropic distance parameter are inadequate for a graben structure with a deep sedimentary trough. A new strategy is devised for the parametrization of attenuation relations in graben structures by looking at the statistical properties of 53 simulated earthquakes of variable magnitudes located at various sites along the western boundary fault of the DSR graben. An exemplary attenuation relation is designed from the synthetics for the 1 Hz spectral acceleration, modifying the Joyner-Boore-type parametrization by adding coefficients suited for three different source-to-sensor configurations: within the graben, beyond the graben and path unaffected by the graben structure.

INTRODUCTION

Prediction of ground motion using well-established methods in seismic hazard assessment (e.g. Cornell, 1968) usually requires attenuation relations. Despite their varying forms (Abrahamson and Silva, 1997, Sadigh et al., 1997, Somerville et al., 1997), all attenuation relations share some engineering ground motion parameters (intensity, peak amplitudes and response spectral values of acceleration, velocity or displacement), which are determined by the magnitude, distance to the earthquake source, and site conditions. A wide breath of relationships and definitions are used for magnitude, distance and site conditions (Campbell, 2003; Douglas, 2003).

2

In general, attenuation relations parameterize distance in a way that does not take into account a change in geological features within the region of interest. This does not necessarily mean that the relations display radial symmetry. For instance, the distance (r_{jb}) parameter proposed by the Joyner-Boore relation (Boore et al., 1997) measures the shortest distance to the (real or projected) surface fault trace and treats the depth as a parameter to be fitted to the data. For a given earthquake with finite fault length, this distance is not constant on a circle around the epicenter but displays a rather elliptical shape (Douglas, 2003).

Sedimentary basins and graben structures, inside which the velocity and the absorption of seismic waves differ from that of the surrounding basement rocks, are types of geological structures that may influence the attenuation of strong ground motion with distance. Both site and basin effects modify the ground motion that can be measured on hard rock, where ideally a frequency-independent amplification of 2 defines the influence of the free surface (for vertically incoming waves). Several features differentiate site effects from basin effects. In terms of size, site effects are limited by engineering seismology practice to the top 30 to a few hundred meters. Whereas site effects are generated by shallow sedimentary features, which may vary significantly laterally, basin effects are controlled by coherent geological structures, which can be correlated over many kilometers laterally and can extend hundreds to thousands of meters at depth. Even though such a structure might also be shallow (i.e. in the case of the Euroseistest site near Thessaloniki in Greece, the sediments reach down to only about 200 m depth, Makra et al., 2001), we focus on deep geological structures such as the Dead Sea basin (DSB).

Site effects, which are frequency-dependent, can range up to a factor of 10 (Bard, 1999), although effects of non-linearity in soft media tend to increase damping, generally reducing amplitudes (Irikura et al., 1998; Anderson, 2002). In the simplest case, these can

be assessed by soil classification schemes and simulated by vertical SH-wave propagation programs such as SHAKE (Schnabel et al., 1972), which includes the assumption of horizontal layering of the strata below the site of interest on the lateral scale of a Fresnel zone. Basin effects are much harder to model and quantify, as they result from focusing and defocusing of waves radiated from earthquake sources. The geological structure which is responsible for the effects must be described by a two- or three-dimensional model. In addition, they also comprise basin edge effects, which are caused by conversion of body to surface waves at the edge of the basin, where the material impedance is maximal. Since this requires consideration of a highly sophisticated wave propagation model, basin effects are not a mere extension of site effects at depth with one-dimensional models.

Basin effects have been observed in a variety of settings, whether in seismic records (Davis et al., 2000, Kawase, 1996) or damage patterns (Tertulliani, 2000, Wust-Bloch, 2002). They have been extensively modeled for some specific areas, such as the Los Angeles Basin (e.g. Olsen, 2000) or the Euroseistest site (e.g. Pitilakis et al., 1999; Makra et al., 2001). However, no attempt so far has been made to incorporate results of 3D modeling of wave propagation in geological structures into the design of attenuation relations. The study described in this paper is an attempt in this direction. In areas such as California and Japan, where abundant acceleration data is available for varying magnitudes, distances, geological areas and site conditions, attenuation relations can be efficiently derived from empirical data and even diversified according to source mechanism as additional parameter (Boore et al., 1997). However, for most earthquake prone zones, such comprehensive databases are not available.

A new approach is proposed here that simulates 3D wave propagation in order to parameterize an attenuation relation for specific types of geological structures. The DSR

area, a typical region with sparse acceleration data, is used to verify the method. Extensive 3D earthquake simulations are utilized to design a strategy for parameterizing attenuation relations inside and around this large scale tectonic structure.

MODEL AND SIMULATIONS

3D modeling of elastic wave propagation generated by an earthquake source has been used to demonstrate the complexity of the wavefield as it evolves in an inhomogeneous medium. The basin-generated focusing and defocusing that is observed in these simulations shows a high degree of wave amplitudes dependence on details of the source process. In reasonably sized 3D models, wave simulations are restricted to frequencies of about 1 Hz, as modeling is usually limited by a lack of knowledge of structural details and computational power.

If the wavelength is used as a scaling parameter, a frequency of 1 Hz is equivalent to 2.3 km wavelength for shear waves with v_S=2.3 km/s, which is the minimum shear wave speed in our model. Thus, speaking about the 3D model used in this study, the results of computations with frequencies beyond 1 Hz could be considered as reasonable only if the structural model would have a better resolution than about 2 – 2.5 km, which clearly is not the case for this model.

This paper investigates basin-generated effects in the Dead Sea region (Figure 1), a zone of sustained seismic activity. Earthquakes with magnitudes between 6.5 and 7.5 have occurred repeatedly throughout historic and prehistoric times (Marco et al, 1996). Due to the continuous settlement of the DSR region, the oldest reports of earthquakes date back to more than 4000 years: Several catalogues have been compiled for large magnitude events (Ben-Menahem, 1991; Ambraseys et al., 1994; Amiran et al., 1994).

Within the Dead Sea region (Figure 1), the Dead Sea Fault System (DSFS) developed into a large N-S trending pull-apart structure characterized by an important topographic depression which comprises the Dead Sea as well as the deep (> 10 km) underlying sedimentary DSB (Ben-Avraham, 1997; Garfunkel and Ben-Avraham, 1996; Ginzburg and Ben-Avraham, 1997). The DSB is a 15 km by 100 km, N-S elongated structure around which basin-related effects have been observed in damage patterns of past earthquakes (Sieberg, 1932; Vered and Striem, 1977; Levy et al., 2000; Wust-Bloch, 2002). These observations corroborate simulated ground motions computed for the 1927 (M_L=6.2) Jericho earthquake (Gottschämmer et al., 2002), which show that wave focusing is significant. The deep sedimentary DSB is observed to act as a wave-guide for seismic loads generated by earthquakes that occur along either of the two boundary faults: The energy radiated into the DSB is higher than the portion radiated into the surrounding crystalline bedrock. In addition, the waves bounce back and forth within the DSB, thereby increasing the overall amplitude of ground motion within the structure, as a large part of the energy radiated into the basin is trapped within the latter one. These investigations also demonstrate that, since the maximal amplitude of potential ground motions is underestimated, the standard relation for amplitude attenuation utilized in regional hazard assessment is inadequate to assess the basin-related effect (due to the trapping of the radiated energy within the basin) of the DSB.

The geological and tectonic features of the DSB (Al-Zoubi et al., 2002, Ben-Avraham, 1997; Garfunkel and Ben-Avraham, 1996) were used to develop a strongly simplified 3D elastic model (compiled by Gottschämmer (2002) following Wust-Bloch, pers. comm.) (Figure 2). The basin, 15×100 km^2 in size, consists of three sedimentary layers that are embedded in crystalline bedrock (v_p=5.5 km/s, v_s=3.2 km/s, ρ=2.7 g/cm^3). The upper layer, which is composed of shales and clastics (v_p=4 km/s, v_s=2.3 km/s, ρ=2.1 g/cm^3)

extends to a depth of 5 km. The two underlying layers, consisting of salt and quartzitic sandstone (v_p=4.5-5 km/s, v_s=2.6-2.9 km/s, ρ=2.3-2.5 g/cm^3), reach out to the maximum depth of 9 km in the center of the DSB. As shown in Garfunkel and Ben-Avraham (1996), the bounding faults of the DSB are dipping very steeply, nearly vertically. Thus, the simplified model of the basin as a narrow trench with vertical boundary faults is an acceptable first order approximation.

The model features were selected to be compatible with the minimal simulation resolution. No material attenuation is included in the simulations. Although the effect of intrinsic attenuation is probably not negligible at frequencies ranging around 1 Hz, its main impact on the simulated ground motion values is to be found at rather remote locations from the source. Estimating an average Q_S-value of 200 (which is considered to represent a reasonable estimation for the area following Cong and Mitchell, 1998), the ground motion amplitudes would be expected to drop by 25-30 % at a distance of 50 km and by about 50 % at a distance of 100 km for a frequency of 1 Hz and the lowest shear wave velocity in our model (2.3 km/s). The unrealistically high shear wave velocity at the surface is due to numerical constraints and makes it impossible to accurately take into account local site effects, which are due to the low seismic velocities of the soft near surface layers (upper 30 to few hundred meters).

Thus, the ground motion values computed here most probably represent an upper bound estimate (especially at larger distances from the source) for (very) hard rock sites. Consideration of material attenuation would lead to a more rapid decrease of the absolute maximum values of ground motion at 1 Hz with distance and thus, the attenuation relation coefficients computed in the next section would be somewhat different, especially leading to a more rapid decay of the predicted ground motion parameters with distance. However, incorporating intrinsic attenuation would affect sites as well within and around the DSB in

a quite similar way and the assessment of the effect that we focus on, namely the trapping of the radiated energy within the DSB (by comparing ground motion predictions within and around the DSB), should not heavily suffer from this simplification.

A 3D staggered-grid finite-difference (FD) scheme (Olsen, 1994) with an accuracy of fourth-order in space and second-order in time is used to carry out the simulations. All of these were computed using a triangular-shaped slip rate function with the rise time being determined through the scaling relation given by Heaton (1990), who came to the conclusion that observed rise times are on the average about one order of magnitude smaller than the time needed for the overall fault to rupture. The seismic moment was calculated with the moment-magnitude scaling relation (Hanks and Kanamori, 1979). Empirical relations between magnitude and rupture length, width and area for strike-slip events (Wells and Coppersmith, 1994) were used to compute the size of each respective rupture area. The rupture front propagates with 70% of the local basin shear wave speed (Geller, 1976) in all simulations and the slip is uniformly distributed on the fault.

Especially the latter assumption is a strong simplification which may have a stronger impact on the modeling results (Graves, 1998). However, this issue is most important if we consider each simulation on its own. If, however, we look at all 53 simulations from the statistical point of view, the effect of a randomly chosen slip distribution for all events (meaning that each event would have a different slip distribution) will most likely only result in slight variations of the coefficients of the attenuation law computed in the following section and a somewhat higher variance. The wave-guide effect of the DSB will nevertheless be present in the simulated ground motions. Since we intend to propose a strategy to parameterize attenuation relations for the DSB area rather than a set of coefficients which shall be applicable for real strong ground motion prediction in the area,

the simplifications concerning the structure and the source are an acceptable first order approximation.

The acceleration data base used for the design of attenuation relations for the DSB region consists of 53 simulations with event magnitudes of 5.5, 6.0, 6.5 and 7.0. All the sources were located along the western boundary fault of the DSB. In order to account for the strong difference in ground motion distribution for earthquakes at different sites, which are mostly due to directivity effects, the rupture planes of all events with the same magnitude taken altogether cover the entire length of the basin edge. 34 simulations were modeled assuming a unilateral rupture process, with the hypocenter being located at a depth of 8 km at the northern respectively southern edge of the rupture plane. The remaining simulations were computed using bilateral rupture processes with the hypocenters located at 8 km depth in the center of the rupture plane. Due to the symmetry of the 3D elastic model for the DSB, simulations only need to be computed for sources generated at one side of the basin. The parameters used for the simulations are compiled in Table 1.

Gottschämmer et al. (2002) simulated the wave propagation for the 1927 Jericho earthquake (M_L=6.2) for frequencies lower than 1.5 Hz. They compared the 1 Hz spectral accelerations with the values computed using the Joyner-Boore attenuation relation (Boore et al., 1997), since it is the attenuation relation presently in use in the area (Hofstetter and Zaslavsky, 2004) and allows frequency-dependent analysis. These investigations demonstrated that the subsurface structure of the DSB (even if it is strongly simplified) is responsible for a strongly heterogeneous spatial distribution of ground motion, with amplifications up to a factor 5 within the basin compared to the values predicted by the Joyner-Boore attenuation relationship (Boore et al.,1997). This is a clear indication that the relation currently in use may be inadequate for the DSB region and that

the geological composition of such a basin should be taken into consideration when designing an attenuation relation.

On the basis of 3D modeling of many earthquakes along the boundary faults of the basin, a new method is designed in order to incorporate the wave-guide effect of the DSB systematically in an attenuation law.

DESIGN OF ATTENUATION RELATIONS FOR THE DSB

The attenuation relations designed are based upon the functional form of the Joyner-Boore (Boore et al., 1997) relations and a parametrization which explicitly accounts for the presence of the DSB structure. The surface of the model is subdivided into three individual regions (Figure 3) that are analyzed independently. Region 1 refers to the zone located outside of the DSB, where the seismic waves can propagate without any interaction with the basin structure. Region 2 corresponds to the zone located beyond the basin relative to the source. Region 3 comprises the interior of the DSB with its sedimentary fill.

For every event that was simulated, about 120 regularly spaced 1 Hz horizontal spectral acceleration values were extracted, leading to a data set of approximately 6400 data points for each of the three regions. Through regression analysis with the one-stage maximum-likelihood method (Joyner and Boore, 1993), we fitted the following equation to the data:

$$\ln Y = b_{1,i} + b_{2,i}(M - 6) + b_{3,i}(M - 6)^2 + b_{4,i} \ln \sqrt{r_{jb}^2 + h^2}$$

where i=1,2,3 refers to a particular region and r_{jb} is the Joyner-Boore distance parameter. The composite relation, whose coefficients are shown in Table 2, includes now a function of a predetermined site characterization. The value of h has been kept constant for the three regions. The attenuation law itself corresponds to the Joyner-Boore relation, but

without the part that accounts for site effects. This term was deliberately ignored because the incorporation of such effects in our simulations would require modeling with slow seismic velocities at the surface (an issue that we discussed earlier) and would result in a much smaller spatial discretization. However, the limitations imposed by computation power and by the resolution of the structural model do not permit to account for site effects caused by the upper 30 or even few hundred meters.

Furthermore, one additional data set covering the complete surface of the model was extracted and a set of coefficients was computed from these data. This approach does not take into account the DSB graben structure and simply corresponds to the Joyner-Boore method, again without the site-dependent term.

Figure 4 shows the computed attenuation relations for a M_W=6.0 event within a distance range of 100 km, which is approximately the maximum source to site distance contained in the data set for region 3 (within the DSB structure). The acceleration values predicted by the attenuation relation for region 3 surpass the values computed for regions 1 and 2 by a factor ranging between 2 and 5 for larger distances. Predictions using the standard Joyner-Boore type relation predict similar values as those obtained by the composite relations for regions 1 and 2, and the latter ones fit into the +/- σ-environment of this isotropic relation. However, predictions for region 3, within the DSB structure, estimate acceleration values that are much higher than those predicted by the isotropic law. Even if one σ is added to the isotropic relation, a similar ground motion level is only reached within the first 15 km in region 3. Thus, at larger distances, even this rather conservative estimate computed with an isotropic attenuation relation fails to reach the 1 Hz acceleration values that would be expected from the composite relation within the DSB. From a statistical point of view, the lower σ-values for the region-dependent relations show that the parametrization selected is reasonable.

In Figure 5, the 1 Hz spectral acceleration values (5% damping) predicted by the different attenuation relations are compared to those calculated by FD-computation for a specific event (M_W=6.0, unilateral rupture to the south). In this case, the surface of the modeling volume has been subdivided in nine distinct smaller strips (Figure 3). Within each strip, the values of all surface grid points with the same N-S extension have been averaged in order to compute acceleration curves along the N-S direction. Outside the DSB, the predictions of both the region-dependent and the isotropic relations are in very good agreement with the data computed with the FD-method. Thus, an isotropic attenuation relation as used presently in the DSB-region seems to be adequate to accurately predict acceleration values in the areas surrounding the DSB. Within the DSB, the situation is very different. The spectral accelerations predicted by the region-dependent relation exhibit a better fit to the FD-values than those proposed by the standard isotropic one, even though in some locations the values computed with the FD-method remain unmatched. However, if one σ is added to the composite relation, the predicted acceleration values fit the simulated data well or lead to a slight overestimation. In that case, more than 92% of the modeled acceleration values can be explained this way.

In order to verify how well the ground motions computed by FD-methods reflect reality, it is indispensable to compare and, if feasible, to calibrate them with real data. In the case of the DSB, an attempt was made to calibrate predictions with strong motion data recorded during the recent M_W=5.2 Northern Dead Sea earthquake of February 11th 2004 (Hofstetter and Zaslavsky, 2004; Wust-Bloch and Joswig, 2004 and submitted), which have been provided by the Geophysical Institute of Israel. Unfortunately, the instrumental coverage of the DSB by the accelerograph array of Israel was insufficient to draw reasonable conclusions concerning the quality of the structural model used, as there was only one single station located within the basin (quite close to the western boundary fault).

CONCLUSIONS

Extensive 3D simulations of earthquakes using a simplified model of the Dead Sea basin (DSB) were used in order to parameterize a composite attenuation relation that takes into account the wave-guiding effects generated by large tectonic features and to check whether or not such a concept might be a suitable alternative to the standard type of attenuation laws (e.g. Boore et al., 1997) currently in use in the area. The simulation of dozens of earthquakes ($5.5 < M < 7.0$) along the boundary faults of the DSB provided a synthetic acceleration database which was utilized to carry out a regression analysis and to compute 1 Hz spectral acceleration attenuation relations.

The parametrization of the composite relation proposed here leads to an improvement of the predicted acceleration values as compared with the ones computed from a standard attenuation relation (type of relation following Boore et al., 1997) with an isotropic distance parameter as presently used in the DSR region. While the ground motion estimation of the latter relation permits to constrain accelerations outside the DSB with acceptable accuracy, it fails to do so within the DSB. A separate treatment of the interior of the basin leads to an improved estimation of acceleration values at sites located within the DSB. Thus, a composite relation which includes different sets of coefficients for the regions located within a basin and those around it presents a reasonable strategy to account for the effects of deep sedimentary basins when assessing seismic hazard.

Since at this stage the composite attenuation relation concept has only been verified for 3D simulations on hard rock sites within a strongly simplified 3D structural model, the next steps include the application of it on real data or the refinement of the structural model and source parametrization of the simulations along with the necessary calibration. This will be the ultimate validation of strong ground motion predictions for basin structures on the basis of this type of composite attenuation relation.

ACKNOWLEGMENTS

REFERENCES

Abrahamson, N.A. and W.J. Silva (1997). Empirical response spectral attenuation relations for shallow crustal earthquakes. Seismol. Res. Lett., 68, 94-128.

Al-Zoubi, A., H. Shulman and Z. Ben-Avraham (2002). Seismic refraction profiles across the southern Dead Sea basin. Tectonophysics, 346, 61-69.

Ambraseys, N.N., C.P. Melville and R.D. Adams (1994). *The seismicity of Egypt, Arabia and the Dead Sea: A historical review.* Cambridge University Press.

Amiran, D.H.K., E. Arieh and T. Turcotte (1994). Earthquakes in Israel and adjacent areas: Macroseismic observations since 100 B.C.E. Israel Exploration Journal, 44, 260-305.

Anderson J. G. (2002). Strong-motion seismology. International Handbook of Earthquake & Engineering Seismology, Part B, (eds. Lee, W. H. K., Kanamori, H., Jennings, P. C. and Kisslinger, C.) Academic Press, Amsterdam, 937-966.

Bard, P.-Y. (1999). Local effects on strong ground motion: Physical basis and estimation methods in view of microzoning studies. Proceedings of the advanced study course

Seismotectonic and microzonation techniques in earthquake engineering: Integrated training in earthquake risk reduction practices, Kefallina.

Ben-Avraham, Z. (1997). Geophysical framework of the Dead Sea, in: *The Dead Sea: The lake and its settings*, Niemi, T.M., Z. Ben-Avraham and J. Gat, eds., 22-35, Oxford University Press, New York.

Ben-Menahem, A. (1991). Four thousand years of seismicity along the Dead Sea Rift. J. Geophys. Res., 96, 20195-20216.

Boore, D.A., W.B. Joyner and T.E. Fumal (1997). Equations for estimating horizontal response spectra and peak acceleration from western North American earthquakes: A summary of recent work. Seismol. Res. Lett., 68, 128-153.

Campbell, K. W. (2003). Strong-Motion Attenuation Relations. in International Handbook of Earthquake and Engineering Seismology, Part B, Academic Press, Amsterdam, 1003-1012.

Cong, L. and B.J. Mitchell (1998). Seismic Velocity and Q Structure of the Middle East Crust and Upper Mantle from Surface-Wave Dispersion and Attenuation. Pure Appl. Geophys., 153, 503-538.

Cornell, C.A. (1968). Engineering seismic risk analysis. Bull. Seismol. Soc. Am., 58, 1583-1606.

Davis, P.M., J.L. Rubinstein, K.H. Liu, S.S. Gao and L. Knopoff (2000). Northridge earthquake damage caused by geological focusing of seismic waves. Science, 289, 1746-1750.

Douglas, J (2003). Earthquake ground motion estimation using strong-motion records: a review of equations for the estimation of peak ground acceleration and response spectral ordinates. Earth Sc. Rev., 61, 43-104.

Garfunkel, Z. and Z. Ben-Avraham (1996). The structure of the Dead Sea basin. Tectonophysics, 266, 155-176.

Geller, R.J. (1976). Scaling relations for earthquake source parameters and magnitudes, Bull. Seismol. Soc. Am., 66, 1501-1523.

Ginzburg, A. and Z. Ben-Avraham (1997). A seismic refraction study of the north basin of the Dead Sea. Geophys. Res. Lett., 24, 2063-2066.

Gottschämmer, E. (2002). Kinematic and dynamic simulation of ground motion: implications for seismic hazard assessment. Cuvillier Verlag Göttingen.

Gottschämmer, E., F. Wenzel, H. Wust-Bloch and Z. Ben-Avraham (2002). Earthquake modeling in the Dead Sea basin. Geophys. Res. Lett., 29, 12, doi: 10.1029/2001GL013800, 8-1 – 8-4.

Graves, R.W. (1998). 3D Finite Difference Modeling of the San Andreas Fault: Source Parameterization and Ground Motion Levels. Bull. Seismol. Soc. Am., 88, 881-897.

Hanks, T.C. and H. Kanamori (1979). A moment magnitude scale. J. Geophys. Res., 84, 2348-2350.

Heaton, T. (1990). Evidence for and implications of self-healing pulses of slip in earthquake rupture. Phys. Earth Planet. Inter., 64, 1-20.

Hofstetter, A. and Y. Zaslavsky (2004). The M_w=5.2 earthquake of February 11 2004 in the Dead Sea basin and assessment of site effects using strong motion data. ESC, XXIX General Assembly, Potsdam, Abstract, p. 9.

Irikura, K., Kudo, K., Okada, H. and Sasatani, T. (Eds.) (1989). "The effects of surface geology on seismic motion." (Proc. of the Second International Symposium on the Effects of Surface Geology on Strong Motions, Yokohama, Japan), Bulkema, Rotterdam.

Joyner, W. and D. Boore (1981). Peak horizontal acceleration and velocity from strong motion records including records from the 1979 Imperial Valley, California, earthquake. Bull. Seismol. Soc. Am., 71, 2011-2038.

Joyner, W.B. and D.M. Boore (1993). Methods for regression analysis of strong-motion data. Bull. Seismol. Soc. Am., 83, 2, 469-487.

Kawase, H. (1996). The cause of the damage belt in Kobe: The Basin-Edge-Effect, constructive interference of the direct S-wave with the basin-induced diffracted/Rayleigh waves. Seismol. Res. Lett., 67, 25-34.

Levy, R., A. Rutenberg, P. Magnus, E. Marianchik and F. Segal (2000). Performance of elevator systems in the 22 November 1995 Gulf of Eilat-Aqaba earthquake, Earthquake Spectra, 3, 607-619.

Makra, K., D. Raptakis, F.J. Chavez-Garcia and K. Pitilakis (2001). Site effects and design provisions: The case of Euroseistest. Pure Appl. Geophys., 158, 12, 2349-2367.

Marco, S., M. Stein and A. Agnon (1996). Long-term earthquake clustering: A 50'000 year paleoseismic record in the Dead Sea graben, J. Geophys. Res. 101, 6179-6191.

Olsen, K.B. (1994). *Simulation of three-dimensional wave propagation in the Salt Lake Basin.* Ph.D. thesis, University of Utah, Salt Lake City.

Olsen, K.B. (2000). Site amplification in the Los Angeles Basin from three-dimensional modeling of ground motion. Bull. Seismol. Soc. Am., 90, 6B, S77-S94.

Pitilakis, K., D. Raptakis, K. Lontzetidis, Th. Tika-Vassilikou and D. Jongmans (1999). Geotechnical and geophysical description of EURO-SEISTEST, using field, laboratory tests and moderate strong motion recordings. J. Earthquake Engineering, 3, 3, 381-409.

Sadigh, K., C.Y. Chang, J.A. Egan, F. Makdisi and R.R. Youngs (1997). Attenuation relationships for shallow crustal earthquakes based on Californian strong motion data. Seismol. Res. Lett., 68, 180-189.

Schnabel, B., J. Lysmer and H.B. Seed (1972). SHAKE. A computer program for earthquake response analysis of horizontally layered sites. College of Engineering, University of California, Berkeley, Report EERC 72-12.

Sieberg, A. (1932). *Untersuchungen über Erdbeben und Bruchschollenbau im östlichen Mittelmeer*, Verlag von Gustav Fischer, Jena.

Somerville, P.G., N.F. Smith, R.W. Graves and N.A. Abrahamson (1997). Modification of empirical strong ground motion attenuation relations to include the amplitude and duration effects of rupture directivity. Seismol. Res. Lett., 68, 199-222.

Tertulliani, A. (2000). Qualitative effects of local geology on damage pattern. Bull. Seismol. Soc. Am., 90, 1543-1548.

Vered, M., and H.L. Striem (1977). A macroseismic study and the implications of structural damage of two recent major earthquakes in the Jordan Rift, Bull. Seismol. Soc. Am., 67, 1607-1613.

Wells, D.L. and K.J. Coppersmith (1994). New empirical relations among magnitude, rupture length, rupture width, rupture area and surface displacement. Bull. Seismol. Soc. Am., 84, 974-1002.

Wust-Bloch, G. H. (2002). The active Dead Sea Rift fault zone: a seismic wave-guide, in Cloetingh and Ben-Avraham eds., EGU, Stephan Müller Special Publication Series, 2, 7-19.

Wust-Bloch, G. H. M. and Joswig (2004). Nanoseismic Monitoring of Aftershocks from the 11 Feb 2004 (ML 5.0) Northern Dead Sea Earthquake, ESC, XXIX General Meeting, Potsdam, Sept 2004 (Abstract) p.12.

Wust-Bloch, G. H. and M. Joswig (submitted). Nanoseismic Monitoring of Aftershocks: Spatial Migration of Short-Term Aftershocks Pulses and Rupture Dynamics.

Table 1. Parameters of the 53 simulations used in this study. The columns contain moment magnitude (M_W), length (L), width (W), hypocentral depth (HD), rise time (τ_R), and the total number of simulations (N) for each magnitude. The number in parentheses near to the total number of simulations for each magnitude is the number of events which have been simulated using a bilateral rupture propagation.

M_W	L [km]	W [km]	HD [km]	τ_R [s]	N
5.5	5.6	5.6	8.0	0.22	26 (9)
6.0	10.0	10.0	8.0	0.39	14 (5)
6.5	21.0	14.0	8.0	0.68	8 (3)
7.0	53.6	14.0	8.0	0.68	5 (2)

Table 2. Coefficients for the 1 Hz spectral acceleration region-dependent attenuation law determined from the synthetic data. The last line contains the coefficients of the isotropic relation.

Region (i)	$b_{1,i}$	$b_{2,i}$	$b_{3,i}$	$b_{4,i}$	σ_i^2
i=1	-2.725	1.759	-0.524	-0.520	0.672
i=2	-2.939	1.950	-0.696	-0.442	0.747
i=3	-1.770	2.078	-0.753	-0.402	0.659
all	-2.052	1.866	-0.712	-0.643	0.826

Figure 1. Topographic map of the Dead Sea region. The outline of the graben and the modeling volume as used for the simulations are indicated as dotted lines.

Figure 2. North-South and East-West cross-sections through the 3D elastic model used for the simulations. The sedimentary basin consists of three layers embedded in crystalline bedrock. The fault plane of the specific event analyzed in Figure 3 and 4 is plotted as a white dashed rectangle and the hypocenter of this simulation is represented by a white cross.

Figure 3. Spatial distribution of 1 Hz spectral acceleration values for the specific simulation considered in Figure 3. The epicenter is represented by a white cross and the rupture plane is indicated with a white line (the rupture propagates to the south). The circled numbers show the three regions that have been analyzed separately in order to compute region-dependent attenuation relations.

Figure 4. Composite (region-dependent) and isotropic attenuation relations (M_W=6.0) for 1 Hz spectral acceleration values determined from our simulations.

Figure 5. Comparison of the spectral accelerations computed for a specific event (solid curve) (see also Figure 3) with the predictions from the region-dependent (dashed line) and isotropic (dotted line) attenuation relations. Adding one σ to the region-dependent relation leads to the dashed-dotted curve. The plots for areas 1 to 3 and 7 to 9 (lower part, outside the basin) are scaled to a lower maximum value than those for areas 4 to 6 (inside the basin).
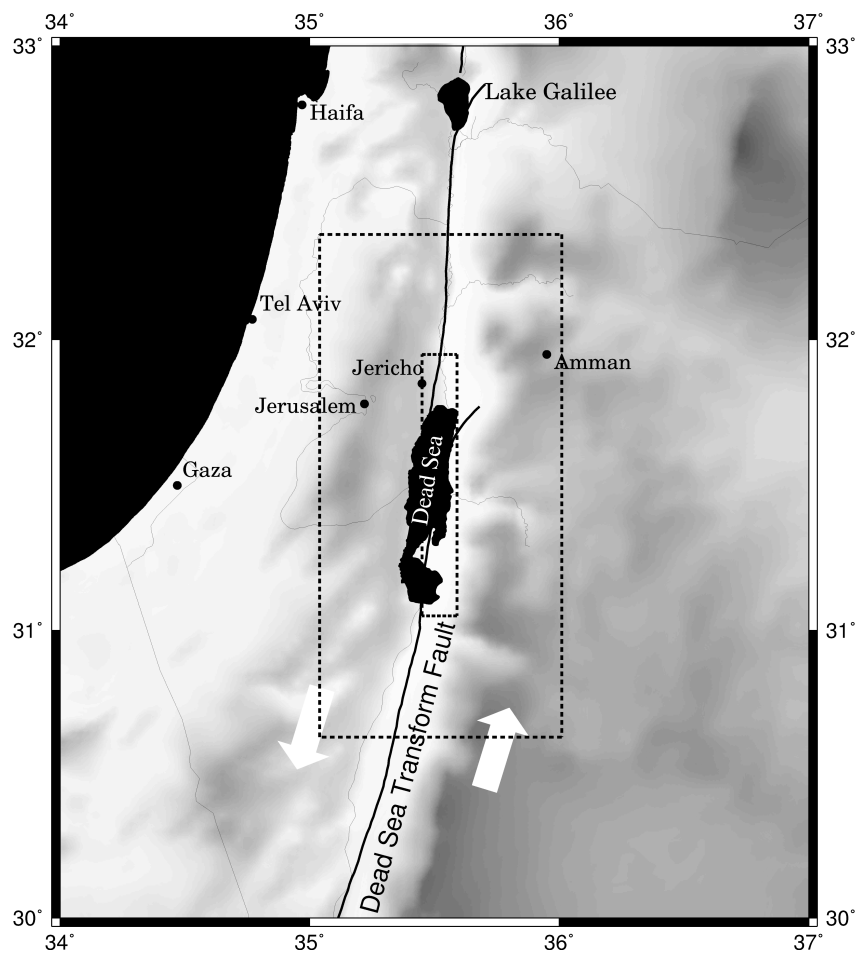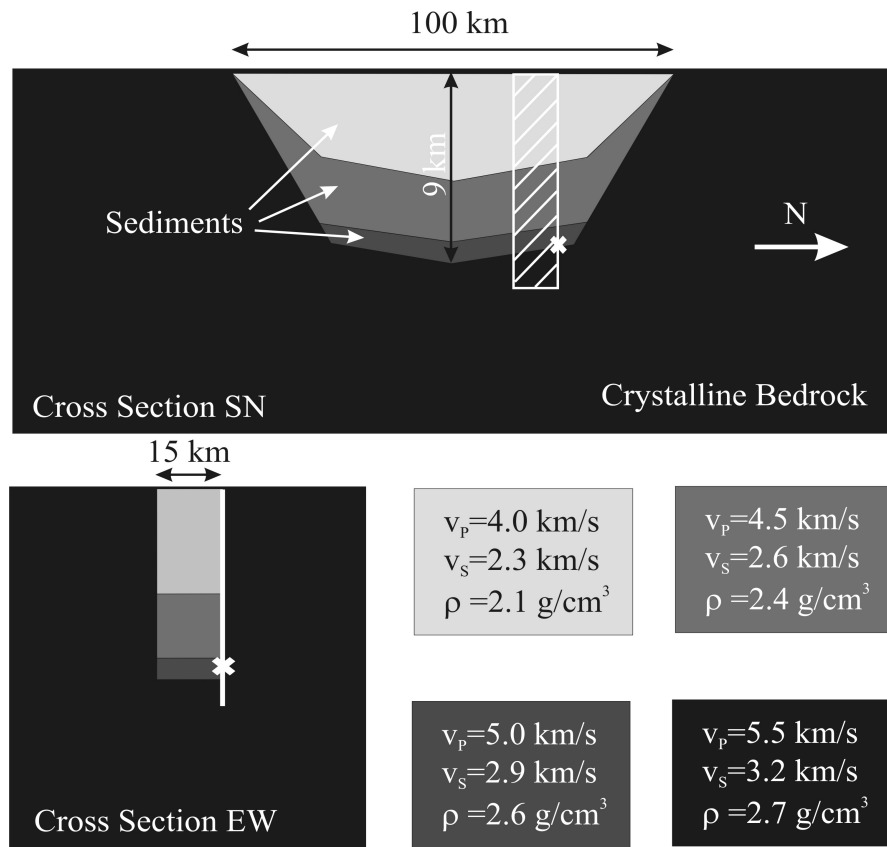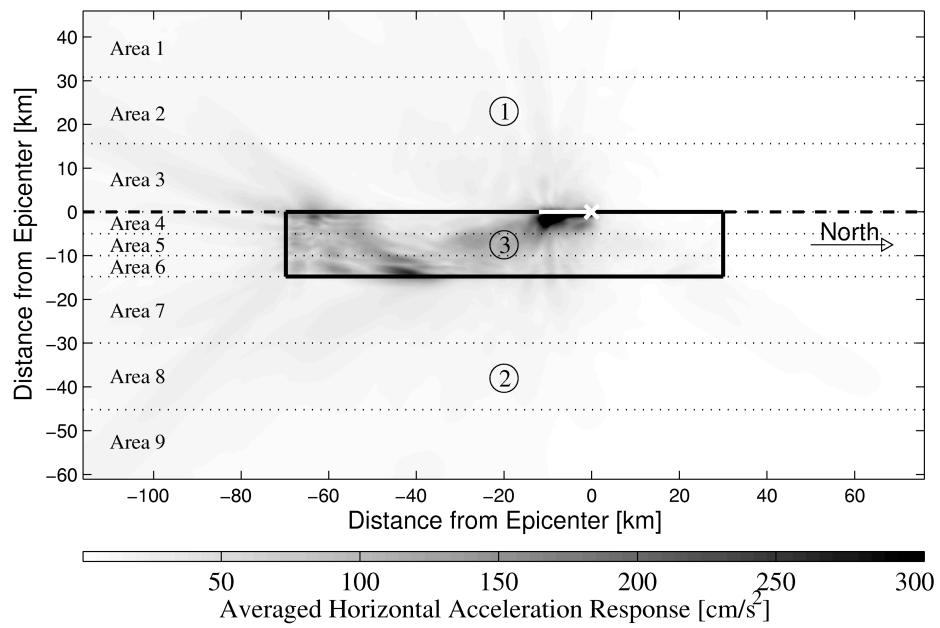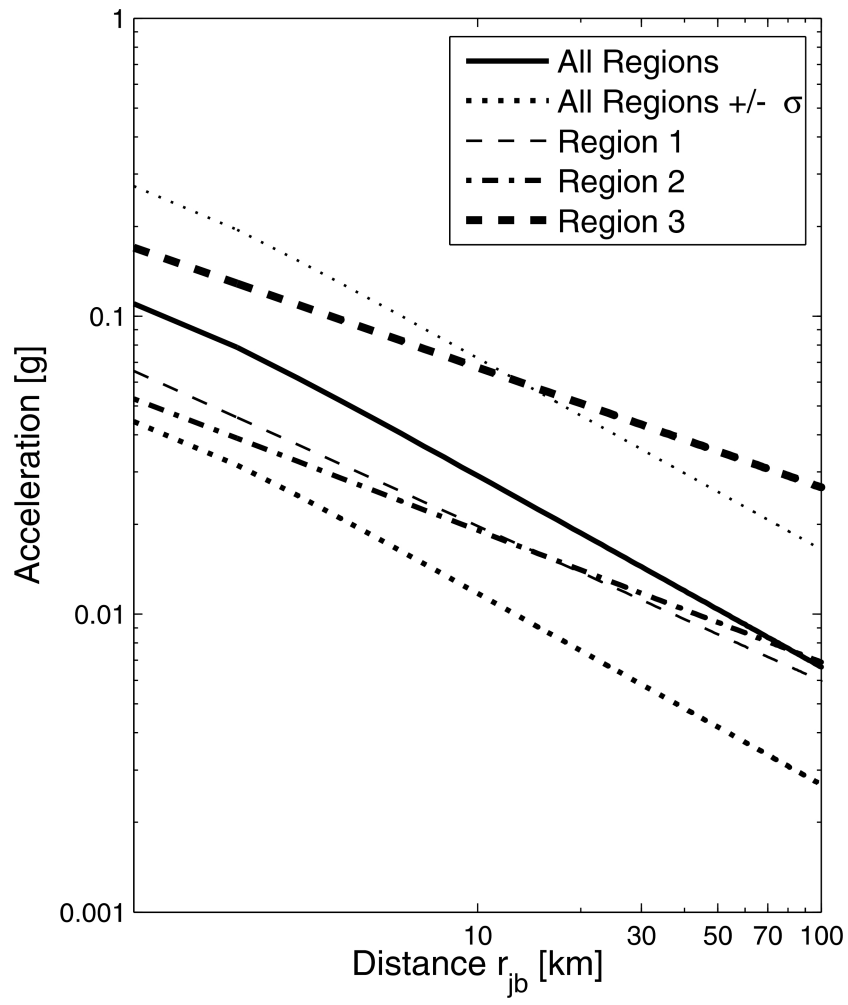
Figure 1

100 km

9 km

Sediments

N

Cross Section SN

Crystalline Bedrock

15 km

v_P=4.0 km/s
v_S=2.3 km/s
ρ =2.1 g/cm^3

v_P=4.5 km/s
v_S=2.6 km/s
ρ =2.4 g/cm^3

v_P=5.0 km/s
v_S=2.9 km/s
ρ =2.6 g/cm^3

v_P=5.5 km/s
v_S=3.2 km/s
ρ =2.7 g/cm^3

Cross Section EW

Figure 2

Averaged Horizontal Acceleration Response [cm/s^2]

Figure 3

Figure 4

Figure 5